IEEE Robotics and Automation Letters (RA-L) paper, presented at ICRA 2026, Vienna, Austria. Cite as RA-L paper.

Fixture-Free Automated Sewing System Using Dual-Arm Manipulator and High-Speed Fabric Edge Detection

Kai Tang, *Graduate Student Member, IEEE*, Xuzhao Huang, *Graduate Student Member, IEEE*, Akira Seino, *Member, IEEE*, Fuyuki Tokuda, *Member, IEEE*, Akinari Kobayashi, *Member, IEEE*, Norman C. Tien, *Senior Member, IEEE*, and Kazuhiro Kosuge, *Life Fellow, IEEE*

***Abstract*—Inspired by human workers who perform complicated sewing tasks by repeating relatively simple operations, this letter proposes a fixture-free automated sewing system using a dual-arm manipulator and an ordinary sewing machine to sew two aligned fabrics along the edges, a common task in garment production. The proposed sewing system has a five-layer architecture: perception, dual-arm sewing Petri net, fundamental operations, control primitives, and hardware layers. This architecture decomposes various complex sewing tasks into sequences of fundamental operations. To meet the real-time requirement of automated sewing, a High-speed Fabric Edge Detection System (Hi-FEDS) is further proposed for the perception layer, which formulates the fabric edge detection problem for sewing as a classification problem of predefined distributed anchors. The anchor distribution is modeled by the Gaussian Uniform Mixture Model (GUMM). This method achieves high-speed fabric edge detection at an average of 120 FPS, with an average error of about one pixel. An experimental robotic sewing platform is developed, and the sewing results show that our system achieves high-quality sewing across fabrics of various shapes and materials.**

***Index Terms*—Bimanual manipulation, deep learning for visual perception, foundations of automation, perception for grasping and manipulation, Petri nets for automation control.**

I. Introduction

GARMENT production consists of various tasks such as fabric cutting, ironing, folding, and sewing. Among these, sewing, a crucial step in garment production, is responsible for about 80% of fabric linkages and accounts for about 40% of the entire production cost [1]. During a sewing task, the skilled workers repeatedly perform a series of operations, including fabric grasping, positioning, aligning, sewing, etc., while ensuring a smooth and precise sewing seam without wrinkles or puckering [2], [3]. Automating this sewing task remains challenging, not only due to the complexities of soft materials manipulation but also because of the real-time and precision requirements of the sewing operation [2].

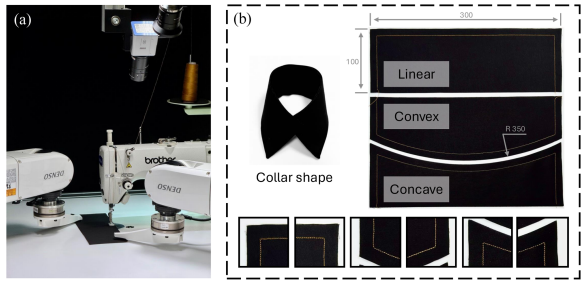

Fig. 1. (a) Experimental robotic sewing platform; (b) Sewing results of fabrics with three different shapes (linear, convex, and concave), with the size of 100 × 300 mm and the curved edge of 350 mm radius. In particular, the collar shape is obtained by turning the concave sewn fabric inside out.

Recent advancements in robotics, control theory, and learning have shown significant potential to facilitate sewing automation. Numerous studies have explored this challenge, including designing mechanisms for fabric handling [4], [5], [6], [7], estimating the desired seams by computer vision [8], [9], modeling the sewing process [10], [11], and manipulating the fabric by using force control [12], [13].

Achieving automated sewing at the level of human workers, sewing without using fixtures [11], however, remains a distant goal. To further advance sewing automation, this letter focuses on two key challenges:

1) Fixture-Free Robotic Sewing System Using Ordinary Sewing Machine: This concerns the sewing of the fabric along the edges without using fixtures [11], ensuring that the seams maintain a consistent distance from the fabric edges, as shown in Fig. 1(b). This is a common task in garment manufacturing to produce items such as collars and cuffs, which cannot be automated without using fixtures. While the existing research in fixture-free sewing [10], [11] has investigated the fundamental process of sewing along a single seam, this letter considers the

Received 19 February 2025; accepted 16 July 2025. Date of publication 23 July 2025; date of current version 29 July 2025. This article was recommended for publication by Associate Editor H. Wang and Editor C.-B. Yan upon evaluation of the reviewers' comments. This work was supported in part by the Innovation and Technology Commission of the HKSAR Government under the InnoHK initiative and in part by the JC STEM Lab of Robotics for Soft Materials, funded by The Hong Kong Jockey Club Charities Trust. *(Corresponding author: Kai Tang.)*

Kai Tang, Xuzhao Huang, Akira Seino, Fuyuki Tokuda, Akinari Kobayashi, and Kazuhiro Kosuge are with the JC STEM Lab of Robotics for Soft Materials, Department of Electrical and Electronic Engineering, Faculty of Engineering, The University of Hong Kong, Hong Kong SAR, China, and also with the Centre for Transformative Garment Production, Hong Kong SAR, China (e-mail: tangkai@eee.hku.hk; xzhuang@eee.hku.hk; akira.seino@transgp.hk; fuyuki.tokuda@transgp.hk; akinari.kobayashi@transgp.hk; kosuge@hku.hk).

Norman C. Tien is with the Department of Electrical and Electronic Engineering, Faculty of Engineering, The University of Hong Kong, Hong Kong SAR, China, and also with the Centre for Transformative Garment Production, Hong Kong SAR, China (e-mail: nctien@hku.hk).

This article has supplementary downloadable material available at https://doi.org/10.1109/LRA.2025.3592145, provided by the authors.

Digital Object Identifier 10.1109/LRA.2025.3592145

IEEE Robotics and Automation Letters (RA-L) paper, presented at ICRA 2026, Vienna, Austria. Cite as RA-L paper.

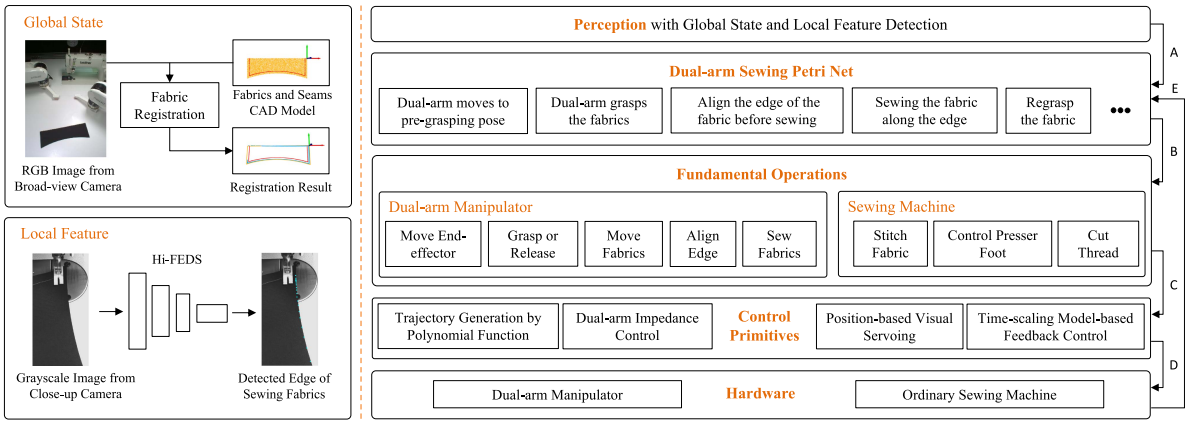

Fig. 2. Fixture-free automated sewing system consists of five layers. The perception layer detects the states of fabrics, denoted as A. The dual-arm sewing Petri net layer generates a series of events, denoted as B, to coordinate the dual-arm manipulator and sewing machine. The generated events are further decomposed into sequences of fundamental operations in the next layer. This fundamental operations sequence, denoted as C, is realized by the combination of control primitives to control the trajectories of end-effectors and the sewing machine. Finally, these trajectories are converted to the command to the hardware, denoted as D. The states of the dual-arm manipulator and sewing machine, denoted as E, are fed back to the upper layer.

automation of complete sewing tasks, which include sewing along multiple seams.

2) Real-Time Estimation of Desired Sewing Seams: Industrial sewing machines can achieve speeds of up to 5000 stitches per minute, about 80 stitches per second [7]. Given the diversity of fabrics and the complexity of the sewing environment, however, no existing system can meet the real-time requirement of the sewing system [10], [11].

To address these challenges, the contributions of this letter are summarized as follows:

- Motivated by the sewing operations of human workers, we propose a fixture-free automated sewing system to sew two aligned fabric parts together along their edges, utilizing a series of fundamental operations of a dual-arm manipulator and an ordinary sewing machine.
- We propose a High-speed Fabric Edge Detection System (Hi-FEDS), which formulates the fabric edge detection problem as a classification problem of distributed anchors. Hi-FEDS meets the real-time requirements of sewing automation while achieving high detection accuracy and robustness.
- We developed an experimental robotic sewing platform. The physical sewing results demonstrate that our system achieves high-quality sewing along the edges across fabrics of various shapes and materials.

The remaining part of this letter is organized as follows: Section II reviews related works. Section III and IV introduce problem statement and problem formulation, respectively. The proposed robotic sewing system is presented in Section V and the proposed Hi-FEDS is introduced in Section VI. Section VII shows the experimental platform and results. Finally, Section VIII concludes the letter.

II. Related Works

A. Robotic Sewing System Development

The complicated sewing process can be decomposed into four basic processes that are SEW, FEED, TENSION, and CONTOUR processes, which is proposed by Gershon et al. [14]. Experimental results showed that this scheme is effective for fundamental sewing operations.

The SEW and FEED processes focus on the cyclic motion of the sewing machine and the feed motion of the robotic system, respectively. Different feeding mechanisms and algorithms are developed to facilitate the sewing and loading [7], [15]. Some research investigated the importance of synchronization between sewing and feed motion [11].

The TENSION process is applied to maintain the fabric shape and to prevent over-stretching. Impedance control [16] and coordinated motion control [17] are widely used to control tension or internal force of the fabrics [12], [13], [18]. Feedback control and visual servoing are applied for the CONTOUR process to sew along the desired seams [3], [10], [19]. However, no existing solution has achieved sewing automation along the fabric edges without using fixtures.

B. Estimation of Desired Sewing Seam

Computer vision is widely used to detect fabric and sewing states during garment production. When there is no real-time requirement, traditional methods such as Random Sample Consensus (RANSAC) and Iterative Closest Point (ICP) are used to detect the position of the fabric [9]. Some research uses deep learning to estimate the desired sewing seams for open-loop sewing trajectory planning [8]. The estimation results of the proposed learning-based methods are more robust than those of traditional computer vision algorithms.

Most of the existing research for edge-tracking sewing uses traditional computer vision algorithms such as Canny and Sobel [19], [20], and heuristic algorithms [3], [15] to detect the fabric edge and estimate the desired sewing seams. Gao et al. [21] formulated the edge detection problem as a fabric segmentation problem and achieved edge detection of 30 FPS and a mean error of 0.61 mm. However, edge detection with higher FPS is essential for high-speed sewing. Recently proposed edge detection networks achieve high mIoU and inference speeds exceeding 150 FPS [22], [23].

III. Problem Statement

This letter proposes a fixture-free automated sewing system employing a dual-arm manipulator and an ordinary sewing machine to detect fabric state and sew along desired seams,

IEEE Robotics and Automation Letters (RA-L) paper, presented at ICRA 2026, Vienna, Austria. Cite as RA-L paper.

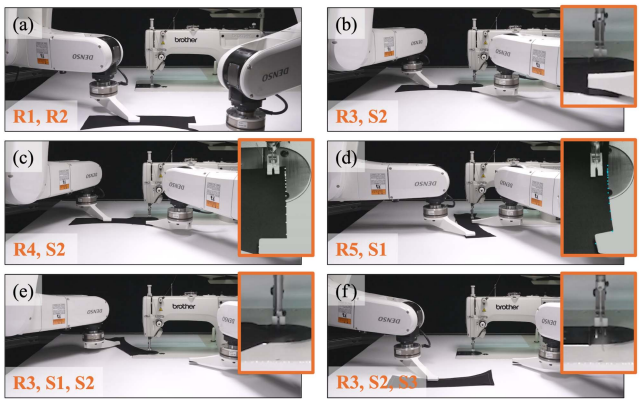

Fig. 3. Examples of the fundamental operations of the automated sewing system. The enlarged figures illustrate the alignment and sewing processes as well as the states of the sewing needle and presser foot.

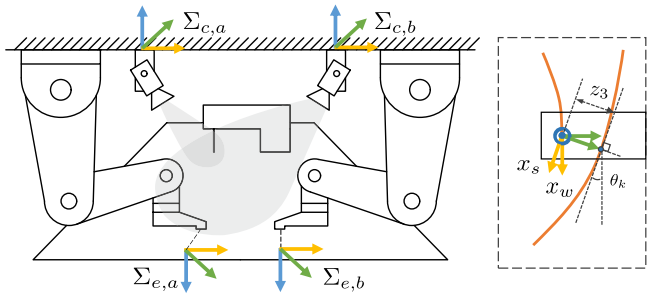

Fig. 4. Coordinate system in this letter with yellow, green, and blue represent the x, y, and z axis, respectively. The shading indicates the field of view of two cameras. The square dash line depicts a top view of the sewing area, with the square solid line as the sewing machine and two orange curve lines as the sewn and desired sewing seam, respectively.

assuming that two fabric pieces are pre-aligned on the table and their CAD models are provided.

The proposed sewing system, as shown in Fig. 2, consists of five layers: perception, dual-arm sewing Petri net, fundamental operations, control primitives, and hardware layers. This system is inspired by human operators who perform a range of complicated sewing tasks by repeating a sequence of relatively simple operations. These operations include grasping fabrics, aligning separated edges; positioning fabrics for sewing; partially flattening the fabrics to be sewn; aligning the fabric edge with the sewing direction; and sewing along the edges. Additionally, the operators utilize the functionalities of the sewing machine, encompassing feeding motion control, presser foot control, and thread cutting.

A. Fundamental Operations of Automated Sewing System

Motivated by this observation, we propose the fundamental operations of a fixture-free automated sewing system, with physical examples shown in Fig. 3. The fundamental operations of the dual-arm manipulator include:

- **R1**: Moving the end-effectors to the target pose without interacting with the environment.
- **R2**: Grasping or releasing fabrics by pressing the end-effector against or lifting it up from the table.
- **R3**: Positioning the fabrics to the target pose.
- **R4**: Aligning the fabric edge to the sewing direction.
- **R5**: Sewing two aligned fabric pieces along the edge.

The fundamental operations of the sewing machine include:

- **S1**: Stitching fabrics by the feeding mechanism.
- **S2**: Controlling the presser foot (lifting or pressing).
- **S3**: Cutting the thread when the sewing task is finished.

IV. Problem Formulation

A. Coordinate Systems

We define the coordinate systems shown in Fig. 4. The feeding direction of the sewing machine is defined as the sewing direction. We define the world frame, Σ_w: $o_w - x_w y_w z_w$, attached to the needle position on the table. x_w is in the opposite sewing direction and z_w is aligned with the upward normal of the table. Additionally, we define the sewing kinematics frame, Σ_s: $o_s - x_s y_s z_s$, with o_s attached to the same location of o_w. x_s is parallel to the tangent line of the desired sewing seam at the point closest to the needle, and z_s is aligned with the upward normal of the table.

We define the end-effector frames, $\Sigma_{e,a}$ and $\Sigma_{e,b}$, attached to the endpoint of each end-effector. Finally, we define two camera coordinate frames, $\Sigma_{c,a}$ and $\Sigma_{c,b}$, which are attached to the close-up and the broad-view cameras, respectively.

B. Modeling and Control of Sewing Process

The kinematics of the sewing process is modeled as a non-holonomic process and is linearized by introducing the time-scaling technique [10] shown as follows:

$$\frac{d}{dz_1}\begin{bmatrix} z_3 \\ z_2 \end{bmatrix} = \begin{bmatrix} 0 & 1 \\ 0 & 0 \end{bmatrix}\begin{bmatrix} z_3 \\ z_2 \end{bmatrix} + \begin{bmatrix} 0 \\ 1 \end{bmatrix}\mu_2, \tag{1a}$$

$$\frac{dz_1}{dt} = \mu_1, \tag{1b}$$

where z_1 is the traveling distance along the desired sewing seam at time t, $z_2 = \tan\theta_k$, where θ_k is the angle between x_w and x_s, and z_3 is the distance between the needle point and the desired sewing seam, as shown in Fig. 4. This system can be stabilized using the control law:

$$\mu_2(z_1) = -K[z_3(z_1),\, z_2(z_1)]^\top, \tag{2}$$

where $K = [k_3,\, k_2] \in \mathbb{R}^2_+$ is the feedback gain.

C. Notation and State Variables

We define the fabric frame Σ_f to represent the fabric pose, assuming that no large deformation occurs during sewing using dual-arm impedance control [11]. The states of the end-effectors are represented by twists $\dot{\boldsymbol{p}}_{e,i} = [\boldsymbol{\omega}_{e,i}^\top, \boldsymbol{v}_{e,i}^\top]^\top \in \mathbb{R}^6$ consisting of angular velocity $\boldsymbol{\omega}_{e,i}^\top \in \mathbb{R}^3$ and velocity $\boldsymbol{v}_{e,i}^\top \in \mathbb{R}^3$, where $i \in \{a, b\}$. The sewing machine is defined as a hybrid dynamic system with continuous state $\dot{\theta}_s \in \mathbb{R}^+$, and discrete states of the presser foot, $p \in \{0, 1\}$, and thread-cutting module, $q \in \{0, 1\}$. $\dot{\theta}_s$ is the angular velocity of the main spindle of the sewing machine. One rotation of the main spindle corresponds to one stitching operation. $p = 0$ and $p = 1$ represent the presser foot down and up, respectively. When $q = 1$, the thread cutting operation is executed.

IEEE Robotics and Automation Letters (RA-L) paper, presented at ICRA 2026, Vienna, Austria. Cite as RA-L paper.

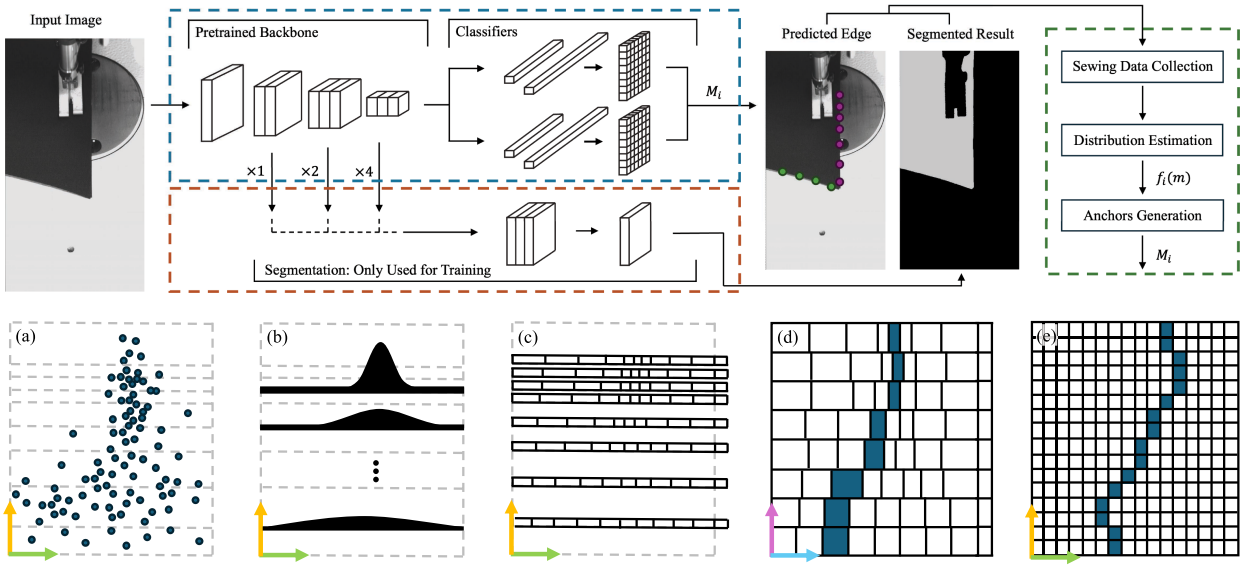

Fig. 5. Upper figure depicts the structure of Hi-FEDS. The main branch is framed by the blue dotted line with a grayscale image as the input and both the vertical and horizontal edges of the fabric as the output. The auxiliary branch is framed by the orange dotted line and data collection module is framed by the green dotted line. The lower figures illustrate the process of modeling the distributed anchors of selected rows for vertical fabric edge detection. (a) The dataset of the appearance of fabric edges observed in real experiments in the image coordinate system; (b) the generated Gaussian-Uniform Mixture Model (GUMM) for each selected rows; (c) the generated anchors for the selected rows, with one more anchor representing no edge is detected in this row; (d) the estimated edge positions of each row in the anchor coordinate system; and (e) an example of an edge in the original image coordinate system. The final two figures demonstrate how Hi-FEDS achieves accurate edge detection while significantly reducing computational complexity.

V. Fixture-Free Automated Sewing System

A. Perception

The global state Σ_f is detected by point cloud registration for grasping point selection. The sewing process state $\boldsymbol{z}$ is estimated for edge alignment and sewing using Hi-FEDS.

For Σ_f, an RGB image of the fabrics captured by the broad-view camera is processed into a binarized map of the aligned fabrics and a binarized map of the edges. Using the intrinsic and extrinsic parameters of the camera, the fabric and edge point clouds are reconstructed. The fabric point cloud is aligned with the fabric CAD model using RANSAC. ICP is then applied to refine the estimation of Σ_f using the edge point cloud and the edge CAD model.

The Hi-FEDS shown in Fig. 5 is applied to detect the edge of fabrics, which is proposed in Section VI. A Kalman filter is then applied to estimate $\boldsymbol{z}$ using the edge information.

B. Dual-Arm Sewing Petri Net and Fundamental Operations

A dual-arm sewing Petri net is developed for discrete event control [24] given the states of fabrics, dual-arm manipulator, and sewing machine. It enables the manipulators to repeat the following events: moving the end-effector to the target pre-grasping pose, grasping the fabric, repositioning the fabric to the target location when necessary, aligning the fabric edge as needed, and sewing along the edges, coordinated with the ordinary functionalities of the sewing machine.

Additionally, using the detected edges by Hi-FEDS, the sewing process is stopped if the curvature of the edge exceeds a certain threshold. The system then rotates the fabrics and realigns the edge to the sewing direction, ensuring a sharp corner in seams, a common requirement in garment production. Further information regarding the proposed Petri net can be found in the supplemental material.

The generated events under different sewing situations are further decomposed into the sequence of relatively simple fundamental operations of the dual-arm manipulator and the sewing machine illustrated in Section III-A. The fundamental operations are implemented using a combination of the predefined control primitives introduced in the next section.

C. Control Primitives and Hardware

1) Trajectory Generation by Polynomial Function: This primitive is used for Move End-Effector and Move Fabrics of fundamental operations shown in Fig. 2. The trajectory of the end-effector or the trajectory of fabrics is generated using a seventh-order polynomial given the initial and target states of the end-effectors or fabrics. By implementing the seventh-order polynomial, the jerk is continuous and the smooth motions of the end-effectors and fabrics are generated.

2) Dual-Arm Impedance Control: This primitive is used for Grasp or Release, Move Fabric, Align Edge, and Sew Fabrics of the fundamental operations, when the end-effector interacts with the environment. It is applied to control the internal force applied to the fabrics and the external force applied to the end-effectors [11]. The control laws for the dual-arm manipulator are shown as follows:

$$\begin{aligned} &\boldsymbol{M}_i \Delta^w \ddot{\boldsymbol{p}}_{e,i} + \boldsymbol{D}_i \Delta^w \dot{\boldsymbol{p}}_{e,i} + \boldsymbol{K}_i \Delta^w \boldsymbol{p}_{e,i} \\ &= \boldsymbol{\Lambda_i} \left({}^w\boldsymbol{W}_{e,i} - {}^w\boldsymbol{W}^d_{e,i} \right), \end{aligned} \tag{3}$$

where $\Delta^w \boldsymbol{p}_{e,i} \in \mathbb{R}^6$ is the displacement of the manipulator i from the nominal state ${}^w\boldsymbol{p}_{e,i}$ in Σ_w. $\Delta^w \dot{\boldsymbol{p}}_{e,i} \in \mathbb{R}^6$ and $\Delta^w \ddot{\boldsymbol{p}}_{e,i} \in \mathbb{R}^6$ are the corresponding twist and acceleration, respectively. $\boldsymbol{M}_i \in \mathbb{R}^{6\times6}$, $\boldsymbol{D}_i \in \mathbb{R}^{6\times6}$, $\boldsymbol{K}_i \in \mathbb{R}^{6\times6}$, are the apparent inertia, damping,

IEEE Robotics and Automation Letters (RA-L) paper, presented at ICRA 2026, Vienna, Austria. Cite as RA-L paper.

and stiffness matrices of end-effector i, respectively. ${}^{w}\boldsymbol{W}_{e,i} = [{}^{w}\boldsymbol{\tau}_{e,i}^{\top}, {}^{w}\boldsymbol{f}_{e,i}^{\top}]^{\top} \in \mathbb{R}^6$ is the wrench applied to the end-effector i, which consists of torque ${}^{w}\boldsymbol{\tau}_{e,i} \in \mathbb{R}^3$, and force ${}^{w}\boldsymbol{f}_{e,i} \in \mathbb{R}^3$. ${}^{w}\boldsymbol{W}_{e,i}^{d} \in \mathbb{R}^6$ is the corresponding desired wrench of manipulator i. $\boldsymbol{\Lambda}_i = \mathbf{diag}(\lambda_1, \lambda_2, \ldots, \lambda_6) \in \mathbb{R}^{6\times6}$ with $\lambda_i \in \{0, 1\}$ is the activation matrix. The impedance law is activated when $\lambda_i = 1$. The twist in $\Sigma_{e,i}$ can be calculated as follows:

$$\Delta\dot{\boldsymbol{p}}_{e,i} = [Ad_{e,iT_w}]\Delta^{w}\dot{\boldsymbol{p}}_{e,i}, \tag{4}$$

where $\Delta\dot{\boldsymbol{p}}_{e,i}$ is represented in $\Sigma_{e,i}$, and $[Ad_{e,iT_w}] \in \mathbb{R}^{6\times6}$ is the adjoint representation calculated as follows:

$$[Ad_{e,iT_w}] = \begin{bmatrix} {}^{e,i}\boldsymbol{R}_w & 0 \\ [{}^{e,i}\boldsymbol{x}_w\times]\,{}^{e,i}\boldsymbol{R}_w & {}^{e,i}\boldsymbol{R}_w \end{bmatrix}, \tag{5}$$

where $[{}^{e,i}\boldsymbol{x}_w\times]$ is the skew-symmetric matrix of the position vector of $\Sigma_{e,i}$ with respect to Σ_w, and ${}^{e,i}\boldsymbol{R}_w \in \mathbb{R}^{3\times3}$ is the rotation matrix of Σ_w with respect to $\Sigma_{e,i}$.

3) Position-Based Visual Servoing: This primitive is used for Align Edge of the fundamental operations using the edge information z_2 and z_3 observed by Hi-FEDS. To ensure the exponential convergence of the system states z_i with $i \in \{2, 3\}$, we design the closed loop dynamics of the linear system (1 a), so that the $\dot{z}_i = -\gamma_i z_i$ holds, where $\gamma_i \in (0, 1)$. The fabrics motion is then represented by a spatial twist ${}^{w}\dot{\boldsymbol{p}}_{vs}(t) = [\boldsymbol{\omega}_{vs}^{\top}(t), \boldsymbol{v}_{vs}^{\top}(t)]^{\top} \in \mathbb{R}^6$, where $\boldsymbol{\omega}_{vs}^{\top}(t) = [0, 0, -\gamma_2 z_2(z_1)]$ and $\boldsymbol{v}_{vs}^{\top}(t) = [-\gamma_2 z_3(z_1) z_2(z_1), -\gamma_3 z_3(z_1), 0]$. z_1 is the traveling distance along the desired sewing seam at time t as shown by (1 b). The end-effector twist is controlled based on the equation:

$$\dot{\boldsymbol{p}}_{e,i} = [Ad_{e,iT_w}]^{w}\dot{\boldsymbol{p}}_{vs}. \tag{6}$$

4) Model-Based Feedback Control: This primitive is used for Sew Edge of the fundamental operations. A control law is applied to generate the angular velocity of the fabric around the needle [10] using the edge information from Hi-FEDS:

$$\omega_s(t) = \frac{-k_2 z_2(z_1(t))\mu_1(t) - k_3 z_3(z_1(t))\mu_1(t)}{1 + z_2(z_1(t))^2}. \tag{7}$$

Besides, the fabrics are fed by the feed dog at a sewing speed v_s calculated by $\dot{\theta}_s$. The whole motion can be represented by a spatial twist ${}^{w}\dot{\boldsymbol{p}}_{fb} = [\boldsymbol{\omega}_{fb}^{\top}, \boldsymbol{v}_{fb}^{\top}]^{\top} \in \mathbb{R}^6$ with respect to Σ_w, where $\boldsymbol{\omega}_{fb}^{\top} = [0, 0, \omega_s]$ and $\boldsymbol{v}_{fb}^{\top} = [0, v_s, 0]$. Then, the twist of each end-effector is controlled by the following equation:

$$\dot{\boldsymbol{p}}_{e,i} = [Ad_{e,iT_w}]^{w}\dot{\boldsymbol{p}}_{fb}. \tag{8}$$

5) Command to Hardware: The calculated twists $\dot{\boldsymbol{p}}_{e,i}$ are then transformed into the joint space velocities of the manipulators. $\dot{\theta}_s = 2\pi v_s / s_s$, with s_s is the stitch size defined by the sewing machine. The command of the dual-arm manipulator and sewing machine is then generated and sent to the hardware in real-time.

VI. High-Speed Fabric Edge Detection System

The High-Speed Fabric Edge Detection System (Hi-FEDS) shown in Fig. 5 is proposed in this section. Unlike the segmentation-based method [21], we reformulate the fabric edge detection problem as a classification problem. This formulation concept has been successfully applied to lane detection to increase the detection speed [25], [26], but higher detection accuracy is needed for fabric edge detection for sewing automation. Hi-FEDS achieves more accurate and robust fabric edge detection by introducing distributed anchors that follow the distribution of the Gaussian Uniform Mixture Model (GUMM) while meeting the real-time requirements of sewing automation.

We first conduct several sewing experiments to collect the image data of the sewing task with the close-up camera. The edges of each image are extracted, and the edge appearance of each image in the image coordinate system is collected as shown in Fig. 5(a). We then select certain rows and columns from the collected edge appearance data. For each row, we estimate a GUMM to represent the distribution of edge appearance shown in Fig. 5(b). After that, we assign a certain number of anchors to each row and column based on the GUMM shown in Fig. 5(c). We then use a classification method to predict the likelihood of the fabric edge appearing in each anchor. The anchor with the maximum likelihood in each row and column is defined as the edge anchor and used to estimate the fabric edge shown in Fig. 5(d).

A. Formulation for Fabric Edge Detection

Let I_{mg} be the captured grayscale image, with dimensions $h \times w$ representing the height and width of the image in the image coordinate system. Subsequently, we select $h_r \in [1, h]$ rows from I_{mg} and assign $w_r \in [2, w+1]$ anchors to each row. We define the anchor with index w_r of each row to represent the case such that no edge appears in that row, resulting in the lower and upper limit of w_r as 2 and $w+1$, as shown in Fig. 5(c), which will be explained later. Similarly, we select $w_c \in [1, w]$ columns and assign $h_c \in [2, h+1]$ anchors to each column. Please note that for each row and column, there is only one edge anchor. When there is no edge appearing in the selected row or column image, the anchor outside of the image will be selected as the edge anchor shown in Fig. 5(c).

Let X be the global feature of I_{mg}. The probability of the fabric edge occurring on each anchor is given by:

$$P_{i,j}^{\kappa} = P(A_{i,j}^{\kappa} = 1|X) = f_{i,j}^{\kappa}(X), \tag{9}$$

where $\kappa \in \{r, c\}$, $1 < i < h_\kappa$, $1 < j < w_\kappa$, A is the event matrix with each item subject to the Bernoulli distribution, and $A_{i,j}^{\kappa} = 1$ represents the event that fabric edge appears at the anchor of i-th rows and j-th column of A^{κ}. $f_{i,j}^{\kappa}$ is defined as the classifier using the global information X.

Let's define the label matrix R^{κ} with the same dimensions as A^{κ}. R_i^r and R_j^c are the one hot labels of the corresponding i-th row of A^r and j-th column of A^c. The optimization problem for obtaining the classifier can then be formulated using the cross-entropy loss as follows:

$$L_{ce} = -\xi_r \sum_{i=1}^{h_r}\sum_{j=1}^{w_r} R_{i,j}^{r} \log P_{i,j}^{r} - \xi_c \sum_{i=1}^{h_c}\sum_{j=1}^{w_c} R_{i,j}^{c} \log P_{i,j}^{c}, \tag{10}$$

where ξ_r and ξ_c are loss weighting factors. By appropriately sampling rows and columns from I_{mg} and assigning anchors to each row and column, we ensure $h_r \ll h$ and $w_c \ll w$ as well as $w_r < w$ and $h_c < h$ shown in Fig. 5. Compared to segmentation-based approaches that classify all pixels, this method significantly reduces the calculation from $h \times w$ to $h_r \times w_r + h_c \times w_c$, enabling the real-time fabric edge detection.

IEEE Robotics and Automation Letters (RA-L) paper, presented at ICRA 2026, Vienna, Austria. Cite as RA-L paper.

B. Distributed Anchors

When the sewing is carried out along the desired seam at a constant distance from the fabric edge, the fabric edge tends to be observed around the area with the constant distance from the needle, as shown in Fig. 5(a). Leveraging this observation, we propose distributed anchors using GUMM to focus computational resources on the area for vertical edge detection, thereby increasing the detection accuracy, compared to assigning the anchor by average sampling along the selected rows, while meeting the real-time requirement of sewing. Note that for the selected columns, the Uniform distribution is applied since we cannot assume any distribution for the horizontal edge of the fabric during sewing.

Besides, since the edge could appear across all columns in the image coordinate system, we combine the Gaussian distribution and the Uniform distribution as GUMM to describe the edge position probabilities. The probability density function (PDF) for each GUMM is expressed as:

$$f_i(m) = \alpha_i \frac{1}{\sqrt{2\pi\sigma_i^2}} \exp\left(-\frac{(m-\mu_i)^2}{2\sigma_i^2}\right) + (1-\alpha_i)\frac{1}{w-1}, \tag{11}$$

where $\alpha_i \in [0,1]$ is the mixing weight, controlling the balance between the Gaussian and Uniform distributions.

Let $n_{i,j} \in \{1,2,\ldots,w_r-1\}$ be the anchor j in i-th selected row and $m_{i,k} \in \{1,2,\ldots,w\}$ be pixel k in i-th selected row. This distribution is then utilized to define the mapping (M_i), from anchor index $(n_{i,j})$ to the pixel index $(m_{i,k})$ using:

$$m_{i,k} = M_i(n_{i,j}) = F_i^{-1}\left(n_{i,j}/(w_r-1)\right), \tag{12a}$$

$$\text{s.t.} \quad : m_{i,k+1} - m_{i,k} \in [1, \Delta m_{\max}], \tag{12b}$$

where $F_i(m_{i,k}) = \int_{-\infty}^{m_{i,k}} f_i(t)\,dt$ is the cumulative distribution function (CDF) of the GUMM, and $\Delta m_{\max}$ is the upper limit of the anchor width to ensure the sufficient resolution of the anchor. This process is illustrated in Fig. 5(b) and (c). The introduction of GUMM enhances detection robustness and accuracy and decreases computational complexity.

Additionally, one extra index is introduced for n_i to account for the possibility of no fabric edge being detected in the i-th row image. As a result, the total number of anchors in each row becomes w_r, ensuring a complete representation of possible edge positions. The same extra index is added to the column anchors to ensure the size of h_c.

C. Network Structure

Hi-FEDS is modeled using a deep neural network shown in Fig. 5. The distribution of anchors is defined based on the real experimental dataset. The global feature X is extracted using a pre-trained backbone, followed by two classifiers (9). Each classifier is modeled by fully connected layers with a dropout layer between them to prevent overfitting. Additionally, an auxiliary branch is introduced as a segmentation-based task to facilitate global feature extraction. Please note that this auxiliary branch is only utilized during training. The overall loss function is given by:

$$L_w = L_{ce} + \xi_{seg} L_{seg}, \tag{13}$$

where L_{seg} is the segmentation loss and ξ_{seg} is the loss weighting factor of the segmentation term.

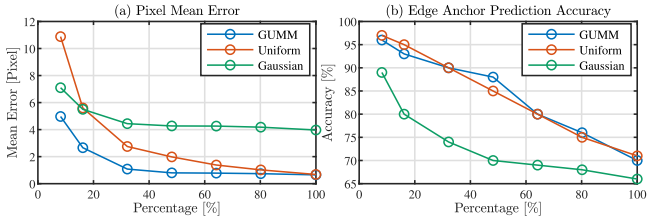

Fig. 6. Evaluation results of Hi-FEDS with anchors generated by different distributions. The horizontal axis shows the number of anchors divided by the number of pixels of selected rows in percent.

VII. Experiments

A. Experimental Platform

An experimental platform shown in Fig. 1(a) has been developed using a dual-arm manipulator system, an ordinary sewing machine, two cameras, and a control PC. Each arm (DENSO VS-068) is equipped with a wrist force and torque sensor (ATI Axia80-M8) with a 3D-printed end-effector. For practical application, a 6 Degree of Freedom (DoF) manipulator can be replaced with a system with fewer DoF.

The ordinary sewing machine (Brother Industries S7100-A) is capable of sewing woven fabrics. The sewing machine motor is replaced by an AC servo motor (Yaskawa Electric SGM7A). The cotton thread with a diameter of about 0.3 mm is used and the stitch size s_s is set to 1.5mm.

The high-speed grayscale camera (Photron INFINICAM UC-1), operating at 624×1246 pixels, provides detailed close-up views of the sewing process, while the RGB camera (Basler acA1920-155uc), with a resolution of 1928×1208 pixels, offers a comprehensive global view. We select and implement the cameras considering their spatial resolution of the camera.

The control PC with an Intel(R) Xeon(R) W-2255 CPU, 64 GB RAM, and an NVIDIA GeForce RTX 3090 GPU has been selected for the control of this system via EtherCAT for the dual-arm manipulator system and the sewing machine, and USB 3.2 for the cameras.

B. Implementation and Training of Hi-FEDS

The dataset was collected with a total of about 10000 images, including fabrics of different shapes and colors, labeled by SAM [27] and adjusted by humans. 80%, 10%, and 10% of the dataset are used for training, validation, and testing, respectively. ResNet-18 is used as the backbone. α_i are selected to satisfied the constraints 12(b). $\Delta m_{\max}$ is defined as 100, corresponding to about 9mm, to ensure the robustness of the edge detection.

The network is trained with PyTorch v2.0.0. We employ an AdamW optimizer with an initial learning rate of 1e-4. The loss weighting factors are set to 1. The batch size is set to 32, and the model is trained for 500 epochs. Data augmentations are applied to prevent over-fitting to the training set. The images are randomly translated and rotated before training.

C. Evaluation of Hi-FEDS

We define two metrics to evaluate the performance of Hi-FEDS: pixel mean error and edge anchor prediction accuracy. The testing dataset, including different fabrics, is used for the evaluation. The pixel mean error is defined as the mean deviation between the predicted vertical edge in selected rows and the

IEEE Robotics and Automation Letters (RA-L) paper, presented at ICRA 2026, Vienna, Austria. Cite as RA-L paper.

TABLE I
COMPARISON OF MEAN FPS AND ERROR OF PURE NETWORK

Method	ENet	SGCPNet	FPENet	PIDNet	**Hi-FEDS**
Mean FPS	185	162	210	238	**308**
Mean Error	1.75	1.50	2.31	1.32	**0.82**

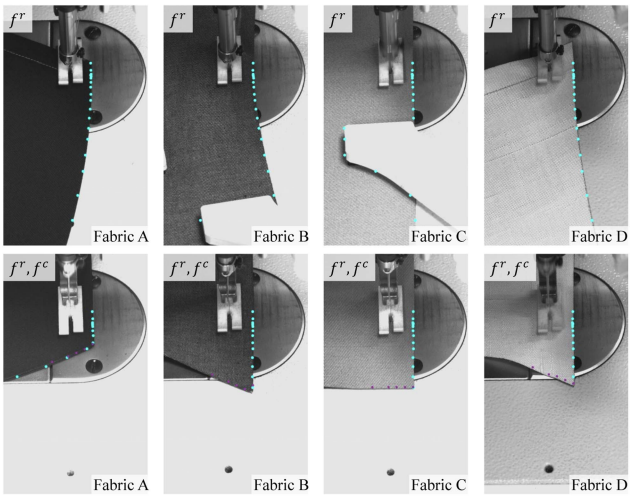

Fig. 7. In the upper row, only $f^r_{i,j}$ is activated to detect the vertical edge, while both $f^r_{i,j}$ and $f^c_{i,j}$ are activated in the lower row as the horizontal edge approaches the sewing needle. This allows Hi-FEDS to detect both vertical and horizontal edges, enabling discrete event control of the transitions between different seam segments to sew seams with a sharp corner.

ground truth in the image. The edge anchor prediction accuracy is given by $N_{ac}/((h_r + w_c)N_{test})$, where N_{ac} is the total number of correct edge anchor predictions and N_{test} is the number of the testing data. The evaluation results are presented in Fig. 6. The pixel mean error using GUMM, Uniform, and Gaussian distributions is shown in Fig. 6(a). As shown in the figure, the prediction result using GUMM outperforms that of using the other distribution for the same number of anchors. Although the edge anchor prediction accuracy using GUMM and Uniform distribution is almost the same as shown in Fig. 6(b). This is because using GUMM assigns more anchors in the regions where edges are more likely to appear. By mapping the predicted edge anchors to the image, the pixel mean error is reduced by about 50%, compared to the Uniform distribution. Additionally, using only Gaussian distributions results in the lowest accuracy. This result occurs because it fails to meet the condition specified in 12(b), namely, that each pixel must correspond to a unique anchor, which directly leads to decreased prediction accuracy.

In particular, using the number of anchors of about 30% of the total number of pixels can achieve nearly the same accuracy as using 100% of the pixels, with an average error of about one pixel for vertical edge detection. As described in the previous Section VI, the Uniform distribution is applied to the column image with the number of anchors equal to about 20% of the number of column pixels. The following experiments are carried out by using this configuration.

Table I compares the inference speed and prediction accuracy of the Hi-FEDS with the state-of-the-art segmentation-based methods shown in [21], [22], [23]. The results show that Hi-FEDS significantly improves both the average FPS and prediction accuracy compared to segmentation-based methods. Note

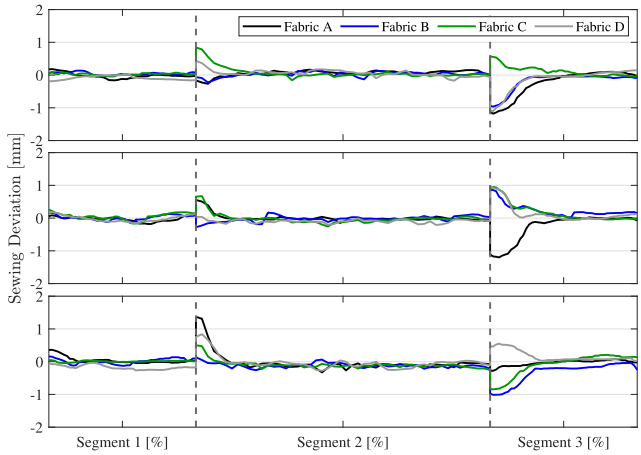

Fig. 8. Numerical sewing results of three sewing tasks using four different types of fabrics. From top to bottom, the experiments utilize fabrics with linear, convex, and concave shapes.

TABLE II
MECHANICAL PROPERTIES OF FABRICS

Properties	Fabric A	Fabric B	Fabric C	Fabric D
Specimen	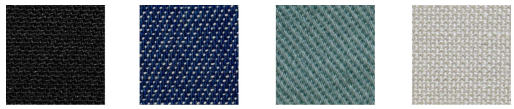			
Material	Cotton	Cotton	Cot.&Poly.	Silk
ρ (kg/m^2)	0.21	0.11	0.18	0.08
T (mm)	0.32	0.25	0.39	0.21
G (N/mm)	0.33	0.25	0.63	0.10
E (MPa)	21.81	9.86	16.46	36.2

ρ:Area Density, T:Thickness, G:Shearing Rigidity, E:Young's Modulus.

that Table I displays the mean FPS of network inference, when including both pre- and post-processing, Hi-FEDS achieves an overall average of about 120 Hz.

D. Experimental Sewing Results

We conduct sewing experiments to demonstrate the fixture-free automated sewing system using fabrics with three different shapes (linear, convex, and concave) and four various materials, as shown in Fig. 1(b) and Table II [28].

For each experiment, two fabrics are aligned and placed on the table. Given the CAD model of the fabrics and desired seams, the proposed system automatically loads the fabrics to the sewing machine, sews the fabrics at a 10 mm distance from the edges, with 10 stitches per second, that is $\dot{\theta}_s = 20\pi$, and finally unloads the sewn fabrics.

The examples of fabric edges detected by Hi-FEDS from the experiments are shown in Fig. 7. Hi-FEDS accurately detects the vertical fabric edge, thus achieving sewing with model-based feedback control. Hi-FEDS also effectively detects the horizontal fabric edge when the fabric corner approaches the needle. The information is fed to the Petri net to facilitate the transition between different seam segments.

Fig. 1(b) shows an example of the sewing results of Fabric A with discontinuous desired seam lines. The sewing results are smooth and even, maintaining a nearly constant distance from the edges of the aligned fabrics. Fig. 8 shows the deviations of

IEEE Robotics and Automation Letters (RA-L) paper, presented at ICRA 2026, Vienna, Austria. Cite as RA-L paper.

the sewn seams from the desired seams of all experiments. The maximum deviation is observed when the fabrics are rotated between two seam segments and is less than the length of one stitch. Furthermore, once the sewing deviation converges, it remains consistently below 0.3 mm. These results highlight the sewing accuracy and robustness of the proposed system.

VIII. Conclusion

This letter proposes a fixture-free automated sewing system that decomposes the entire sewing task into a sequence of the fundamental operations of the dual-arm manipulator and an ordinary sewing machine. To meet the real-time sewing requirements, the Hi-FEDS is proposed, which enables high-speed fabric edge detection with high accuracy and robustness for real-time edge-tracking sewing. Experimental results show the high-performance of sewing using fabrics with diverse shapes and materials (e.g., collar components common in garment production), and indicate its significant potential for industrial application.

Future work will focus on improving the proposed system by incorporating an automated fabric stacking and alignment system, thereby eliminating the current assumption.

References

[1] T. Gries and V. Lutz, "8 — Application of robotics in garment manufacturing," in *Automation in Garment Manufacturing* (The Textile Institute Book Series). Cambridge, U.K.: Woodhead Publishing, 2018, pp. 179–197.

[2] P. M. Taylor and D. M. Pollet, "Why is automated garment manufacture so difficult?," in *Proc. 8th Int. Conf. Adv. Robot.*, 1997, pp. 39–44.

[3] N. Kosaka, Y. Chida, M. Tanemura, and K. Yamazaki, "Real-time optimal control of automatic sewing considering fabric geometric shapes," *Mechatronics*, vol. 94, 2023, Art. no. 103005.

[4] J. Borràs, G. Alenyà, and C. Torras, "A grasping-centered analysis for cloth manipulation," *IEEE Trans. Robot.*, vol. 36, no. 3, pp. 924–936, Jun. 2020.

[5] S. Ku, J. Myeong, H.-Y. Kim, and Y.-L. Park, "Delicate fabric handling using a soft robotic gripper with embedded microneedles," *IEEE Robot. Autom. Lett.*, vol. 5, no. 3, pp. 4852–4858, Jul. 2020.

[6] H. -T. Lin, "Development of the intelligent pneumatic sewing platform for mask production," *IEEE Access*, vol. 8, pp. 141777–141786, 2020.

[7] R. C. Winck, S. Dickerson, W. J. Book, and J. D. Huggins, "A novel approach to fabric control for automated sewing," in *Proc. IEEE/ASME Int. Conf. Adv. Intell. Mechatron.*, 2009, pp. 53–58.

[8] S. Ku, H. Choi, H. -Y. Kim, and Y. -L. Park, "Automated sewing system enabled by machine vision for smart garment manufacturing," *IEEE Robot. Autom. Lett.*, vol. 8, no. 9, pp. 5680–5687, Sep. 2023.

[9] S. Lee et al., "Implementation of an automated manufacturing process for smart clothing: The case study of a smart sports bra," *Processes*, vol. 9, 2021, Art. no. 289.

[10] K. Tang, F. Tokuda, A. Seino, A. Kobayashi, N. C. Tien, and K. Kosuge, "Time-scaling modeling and control of robotic sewing system," *IEEE/ASME Trans. Mechatron.*, vol. 29, no. 4, pp. 3166–3174, Aug. 2024.

[11] F. Tokuda, R. Murakami, A. Seino, A. Kobayashi, M. Hayashibe, and K. Kosuge, "Fixture-free 2D sewing using a dual-arm manipulator system," *IEEE Trans. Autom. Sci. Eng.*, vol. 22, pp. 7927–7940, 2025.

[12] F. Li, D. Hou, J. Song, W. He, and R. Song, "Research on robot sewing method based on process modeling," *Int. J. Intell. Robot. Appl.*, vol. 8, pp. 401–421, 2024.

[13] D. Triantafyllou, P. N. Koustoumpardis, and N. A. Aspragathos, "Model reference fuzzy learning force control for robotized sewing," in *Proc. Mediterranean Conf. Control Autom.*, 2011, pp. 1460–1465.

[14] D. Gershon, "Parallel process decomposition of a dynamic manipulation task: Robotic sewing," *IEEE Trans. Robot. Autom.*, vol. 6, no. 3, pp. 357–367, Jun. 1990.

[15] T. Shungo and D. Hisashi, "Development of fabric feed mechanism using horizontal articulated dual manipulator for automated sewing," in *Proc. 17th Int. Conf. Automat. Sci. Eng.*, 2021, pp. 1832–1837.

[16] N. Hogan, "Impedance control: An approach to manipulation," in *Proc. Amer. Control Conf.*, 1984, pp. 304–313.

[17] K. Kosuge and Y. Hirata, "Coordinated motion control of multiple manipulators," in *Robotics and Automation Handbook*. Boca Raton, FL, USA: CRC Press, 2018, pp. 399–410.

[18] J. Schrimpf and G. Mathisen, "Differential feed control applied to corner matching in automated sewing," in *Proc. Int. Conf. Robot. Automat.*, 2016, pp. 3894–3900.

[19] P. T. Zacharia, "An adaptive neuro-fuzzy inference system for robot handling fabrics with curved edges towards sewing," *J. Intell. Robot. Syst.*, vol. 58, pp. 193–209, 2010.

[20] W. -K. Jung et al., "Appropriate smart factory for SMEs: Concept, application and perspective," *Int. J. Precis. Eng. Manuf.*, vol. 22, pp. 201–215, 2021.

[21] X. Gao, Q. Lizhe, M. Chuangjia, and Y. Sun, "Research on real-time cloth edge extraction method based on ENet semantic segmentation," *J. Engineered Fibers Fabrics*, vol. 17, 2022, Art. no. 15589250221131890.

[22] S. Hao, Y. Zhou, Y. Guo, R. Hong, J. Cheng, and M. Wang, "Real-time semantic segmentation via spatial-detail guided context propagation," *IEEE Trans. Neural Netw. Learn. Syst.*, vol. 36, no. 3, pp. 4042–4053, Mar. 2025.

[23] J. Xu, Z. Xiong, and S. P. Bhattacharyya, "PIDNet: A real-time semantic segmentation network inspired by PID controllers," in *Proc. IEEE Comput. Soc. Conf. Comput. Vis. Pattern Recognit.*, Jun. 2023, pp. 19529–19539.

[24] I. Grobelna and A. Karatkevich, "Challenges in application of Petri nets in manufacturing systems," *Electronics*, vol. 10, no. 18, 2021, Art. no. 2305.

[25] Y. Zhang, Z. Lu, X. Zhang, J.-H. Xue, and Q. Liao, "Deep learning in lane marking detection: A survey," *IEEE Trans. Intell. Transp. Syst.*, vol. 23, no. 7, pp. 5976–5992, Jul. 2022.

[26] Z. Qin, P. Zhang, and X. Li, "Ultra fast deep lane detection with hybrid anchor driven ordinal classification," *IEEE Trans. Pattern Anal. Mach. Intell.*, vol. 46, no. 5, pp. 2555–2568, May 2024.

[27] A. Kirillov et al., "Segment anything," in *Proc. IEEE/CVF Int. Conf. Comput. Vis.*, 2023, pp. 3992–4003.

[28] S. Kuijpers, C. Luible-Bär, and R. Gong, "The measurement of fabric properties for virtual simulation—A critical review," IEEE Standards Association, Industry Connections Report, 1-43, Feb. 2020.